Progress In Electromagnetics Research C, Vol. 68, 45–55, 2016

High-Gain Planar Lens Antennas Based on Transformation Optics and Substrate-Integrated Waveguide (SIW) Technology

Iman Aghanejad[1, *], Habibollah Abiri[2], and Alireza Yahaghi[2]

Abstract—Transformation of space coordinates is a tool to synthesize material properties in view of obtaining a controlled electromagnetic field pattern. Also, substrate-integrated waveguide (SIW) technology can well be exploited to develop microwave and millimeter-wave components. In this paper, by combining these features, high-gain SIW planar lens antennas are proposed. Using the embedded transformation-optics lenses, both narrow beamwidth of 12° and low sidelobe levels of −23 dB are achieved for the H-plane radiation patterns by a single antenna. The designed transformation-optics lenses can be realized by drilling spatially varying cylindrical holes in an ordinary dielectric substrate. The E-plane radiation patterns can also be improved through the dielectric slabs in front of the antenna aperture integrated in the same substrate. Therefore, using SIW technology, the lens antennas can be fabricated on a single substrate. An H-plane sectoral horn and a Maxwell-fisheye-based lens antenna are designed using the proposed method. Simulation results confirm the validity of the proposed idea and the advantages of these lens antennas.

1. INTRODUCTION

The theory of transformation optics (TO) was introduced by independent works of Pendry et al. [1] and Leonhardt [2]. Based on this technique, a methodology has been established for manipulating the electromagnetic waves propagation by assigning material spatial properties. Therefore, TO theory together with metamaterial technology has been intensively explored in various structures such as cloaks [3, 4], perfect lenses [5, 6], and concentrators [7]. In addition, making use of this powerful technique has led to new types of antennas [8–12].

Unfortunately μ and ε tensors obtained using the general TO theory are usually so complicated that they cannot be realized easily [13]. Furthermore, resonant behavior of metamaterials in these structures causes narrow bandwidth of operation and unavoidable losses which in turn limit the practical applications of the design method. To address the problem, a TO design procedure based on conformal and quasi-conformal mapping was proposed and successfully applied in various designs [14–20]. In [21] and [22], using a conformal and a quasi-conformal transformation, the design approach of an H-plane sectoral horn and a Maxwell-fisheye-based lens antenna with high gains and low sidelobes were proposed by the authors which could be realized by isotropic graded refractive index materials.

Substrate-integrated waveguide (SIW) has proved to be a promising technology for the development of microwave and millimeter-wave components. SIWs are integrated waveguide-like structures fabricated by embedding two rows of conducting cylinders in a dielectric substrate, through which two parallel metal plates are electrically connected. In this way, one can implement the non-planar rectangular waveguide in planar form, where the existing planar processing techniques may be applied. SIW structures and classical rectangular waveguides have similar propagation characteristics, such as the

Received 8 July 2016, Accepted 19 September 2016, Scheduled 5 October 2016

* Corresponding author: Iman Aghanejad (i.aghanejad@gmail.com).

[1] School of Engineering, The University of British Columbia, Kelowna, British Columbia, Canada. [2] School of Electrical and Computer Engineering, Shiraz University, Shiraz, Iran.

field pattern and dispersion characteristics. SIW structures also maintain most of the advantages of conventional waveguides, namely self-consistent electrical shielding. However, the salient advantage of the SIW technology is its capability to integrate all of the required components including passive and active elements and even antennas on the same substrate. As the technical literature shows, most of the classical waveguide components have been implemented in SIW technology [23]. Recently, the interest in SIW-based antennas has increased considerably and several structures have been proposed [24–27]. In [28], an H-plane sectoral horn antenna in SIW technology was proposed, where it was also combined with a dielectric loading integrated in the same substrate. The dielectric slab loaded in front of the horn aperture can be considered as a dielectric guiding structure which is excited by the horn aperture, resulting in high gain and narrow beamwidths in both E- and H-plane. In addition, an array formed by four SIW antennas and 5-way power divider as the feed network has been used to obtain higher gain.

In this paper, using transformation optics and SIW technology, a high-gain H-plane sectoral horn and a Maxwell-fisheye-based lens antenna are presented. Using transformation optics as a powerful design tool, the H-plane radiation patterns are manipulated via embedded lenses and high-gains with narrow beamwidths, and low sidelob levels have been achieved with single lens antennas. The designed lenses can be realized using two-dimensional graded photonic crystals (GPCs). The two-dimensional graded photonic crystals consist of spatially varying cylindrical holes drilled in a dielectric host. The E-plane radiation patterns can also be improved through the dielectric slabs in front of the antenna aperture integrated in the same substrate. Therefore, using SIW technology, the lens antennas can be realized using a single substrate. Simulation results of the designs are presented to confirm the validity of the proposed idea and the advantage of these lens antennas.

2. DESIGN OF THE H-PLANE HORN LENS ANTENNA WITH HIGH GAIN AND LOW SIDELOBES

In order to design the horn lens antenna at the operating frequency of 35 GHz using gradient index metamaterials, Figure 1(a) in the virtual space is conformally mapped to the horn shown in Figure 1(c) according to [21]. With this mapping and using transformation optics, the distribution of proper refractive index for converting the quasi-cylindrical waves (generated by the 2D horn) to plane waves which produces a directive beam, is calculated. The dimensions of Figure 1(a) are: $a = 3.77\,\text{mm}$, $b = 60\,\text{mm}$, and $L = 44.18\,\text{mm}$, and the arc length AD is found to be 65.04 mm. In the horn of Figure 1(c), $a = 3.77\,\text{mm}$, $b' = 65.04\,\text{mm}$ (where b' is the same as the arc length AD in virtual space), and $L'' = 51\,\text{mm}$ to have the same conformal module (M) as that of the virtual domain. Using a rectangular intermediate domain with $a = 3.77\,\text{mm}$ and $L' = M \cdot a$ as shown in Figure 1(b), the refractive index of the lens ($n(x, y)$) can be calculated in two steps of mapping. In the first step, by

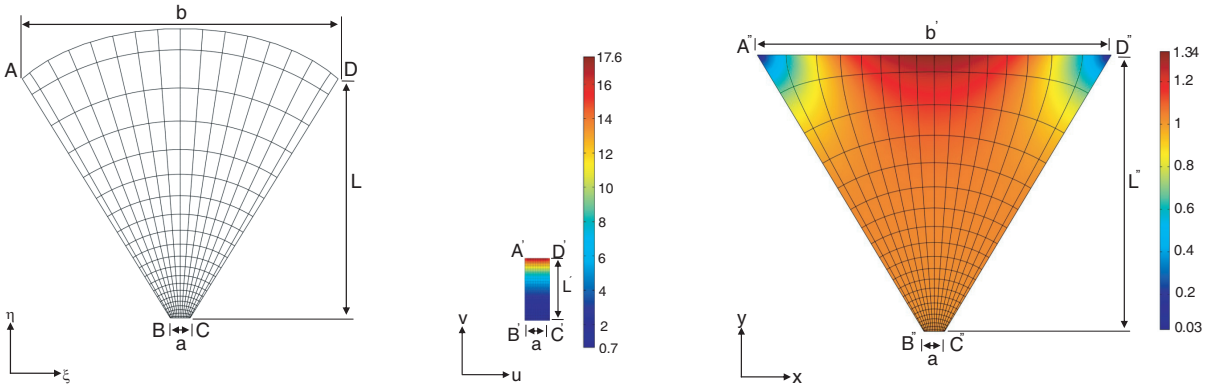

(a) (b) (c)

Figure 1. Steps of conformal mapping. (a) The determined quadrilateral in virtual free space. (b) The rectangle in the intermediate space. (c) The lens antenna resulting from conformal mapping.

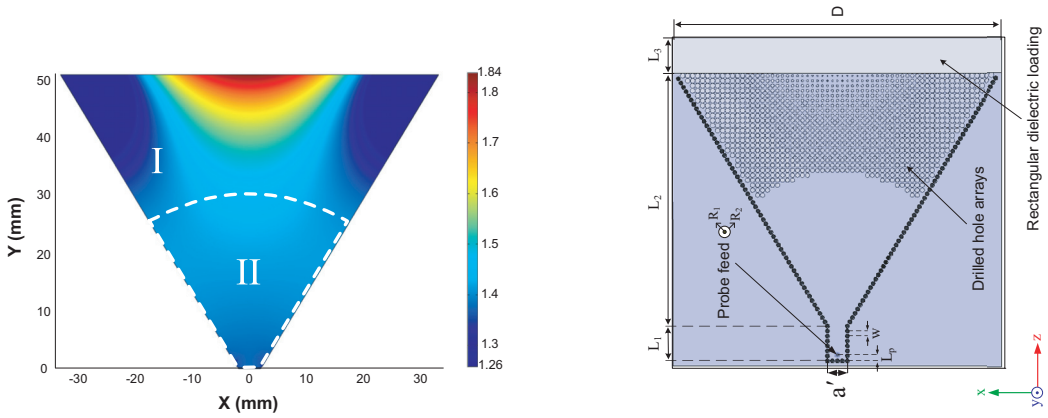

(a) (b)

Figure 2. (a) Profile of the refractive index for the proposed non-dispersive lens antenna. The index values in region II vary smoothly and are roughly equal to 1.4. (b) Structure of SIW horn lens antenna with a rectangular dielectric loading. $W = 1\,\text{mm}$, $a^{'} = 4\,\text{mm}$, $L_1 = 7\,\text{mm}$, $L_2 = 50.83\,\text{mm}$, $L_3 = 7.1\,\text{mm}$, $L_p = 1.23\,\text{mm}$, $D = 66\,\text{mm}$, $R_2 = 0.5\,\text{mm}$, $R_1 = 0.25\,\text{mm}$. The thickness of the dielectric substrate is 2.439 mm.

conformally mapping the virtual domain into the intermediate domain, the material for transformation $(n^{'}(u,v))$ is obtained in the intermediate domain. In the second step, the physical domain is conformally mapped into the intermediate domain so that using the obtained material for the intermediate space in step 1, the refraction indices in the physical domain are calculated. The first mapping step can be obtained by solving the following Laplace's equations for analytical functions $u(\xi,\eta)$ and $v(\xi,\eta)$ in the virtual space:

$$u_{\xi\xi} + u_{\eta\eta} = 0, \qquad v_{\xi\xi} + v_{\eta\eta} = 0, \tag{1}$$

subject to the following boundary conditions:

$$u|_{AB} = -1.88, \quad u|_{CD} = 1.88, \quad n.\nabla u|_{BC,AD} = 0 \tag{2}$$

$$v|_{BC} = 0, \quad v|_{AD} = M \cdot a, \quad n.\nabla v|_{AB,CD} = 0 \tag{3}$$

where n is the outward normal to the surface boundaries, and the conformal module M is given by $M = (1/a)\int_{CD} |\partial u/\partial n| ds$ [29]. A CAD tool like COMSOL [30] can be used for calculating the solution. Once the solutions are known, noting that the virtual domain is empty ($\varepsilon_r = 1$), first the dielectric properties of the intermediate domain can be calculated using $n^{'}(\xi,\eta) = 1/\sqrt{u_\xi^2 + u_\eta^2}$ in the virtual domain. Then, by interpolation, $n^{'}(u,v)$ is determined in the intermediate domain as shown in Figure 1(b). The second mapping step can be obtained by solving the following Laplace's equations for analytical functions $u(x,y)$ and $v(x,y)$ in the physical space:

$$u_{xx} + u_{yy} = 0, \qquad v_{xx} + v_{yy} = 0, \tag{4}$$

subject to the following boundary conditions:

$$u|_{A''B''} = -1.88, \; u|_{C''D''} = 1.88, \; n.\nabla u|_{B''C'',A''D''} = 0 \tag{5}$$

$$v|_{B''C''} = 0, \quad v|_{A''D''} = M \cdot a, \quad n.\nabla v|_{A''B'',C''D''} = 0 \tag{6}$$

When the solution is obtained, using the dielectric properties of the intermediate domain $(n^{'}(u,v))$, the final index in the physical domain is calculated as:

$$n(x,y) = n^{'}(u,v) \times \sqrt{u_x^2 + u_y^2}. \tag{7}$$

The distribution of the refractive index for the designed lens is shown in Figure 1(c). The grid lines indicate the applied conformal mappings between the regions in Figure 1. It is seen that the index

varies between 0.03 and 1.34. The variation is greater in the opening part of the horn, with larger and smaller values in the center and around the two corners, respectively. In most parts of the lens, the index varies smoothly and is roughly equal to 1. However, there exist dispersive (less than unity) values as well.

3. LENS ANTENNA IMPLEMENTATION

As will be shown in Section 3.1, by applying proper simplifying techniques, the designed lens can be easily realized using planar PCB boards. In this study, a substrate with a dielectric constant of 3.38, a loss tangent of 0.0027 and a thickness of 2.439 mm is used. In order to realize the lens, the method presented in [31] is applied. It is a general technique to realize isotropic graded refractive index media using two-dimensional graded photonic crystals. Finally, in Section 3.2, by applying the method proposed in [28], the horn lens antenna is realized by a single substrate using the SIW technology.

3.1. Lens Implementation Using Graded Photonic Crystals

Gradient index materials can be realized using two-dimensional graded photonic crystals. Two-dimensional GPCs are composed of spatially varying cylindrical air holes, drilled in a dielectric host. Since the working wavelength is larger than the size of the holes in the host medium, GPCs are considered as effective media [32]. Therefore, effective medium theory can be applied, and the overall electromagnetic property of the composite material can be described by varying the effective index. Under the quasi-static condition, the following formula applies very well for TE polarization (the electric field is parallel to the axes of the cylindrical holes), and was used to analytically calculate the holes radii [32]:

$$\varepsilon = f + \varepsilon_d(1 - f) \tag{8}$$

where ε_d is the dielectric constant of the substrate, and f denotes the volume fraction of the holes. By changing the radii of the holes r and hence the volume fraction f, different permittivities for the distribution of the gradient index materials can be obtained.

Here each hole is placed in a 1 by 1 mm^2 cell in the substrate with $\varepsilon_d = 3.38$. Using Equation (8), it is easy to obtain the refractive index for a medium, which varies from 1.26 ($r = 0.49$ mm) to $\sqrt{3.38} \simeq 1.84$ ($r = 0$). In order to implement the designed lens in Section 2, first, all refractive index values of the lens profile ($n_{\min} = 0.03, n_{\max} = 1.34$) are multiplied by 1.37 (1.84/1.34) and then, all the less-than 1.26 values are replaced by 1.26 so that the required refractive index lies in the interval. The obtained non-dispersive refractive index profile, with greater than unity values, is shown in Figure 2(a). As can be seen, the index values in region II vary smoothly and are roughly equal to 1.4. In order to simplify the realization of this lens, we may further simplify the profile by replacing all values of the refractive indices in region II by 1.84 which is the index of the substrate. The achieved refractive index distribution is referred to as the simplified non-dispersive profile and used in the implementation of the SIW horn lens antenna.

Using COMSOL CAD tool which is a full-wave solver based on the Finite Element Method [30], the performance of the proposed lens antennas excited by the TE_{10} mode of a dielectric-filled waveguide with the width $a = 3.77$ mm and refractive index 1.84 has been investigated at the working frequency 35 GHz. Simulation results for the far-field radiation patterns in Figure 3 show that these simplifications lead to higher, however, acceptable sidelobe levels. The half-power beamwidth (HPBW) and peak sidelobe ratio (PSLR) of the non-dispersive lens antenna are 11.53° and -19.3 dB, respectively. In addition, corresponding reflection analyses demonstrate that wideband matching can be achieved for the simplified non-dispersive lens in which the refractive index discontinuity between the lens and dielectric-filled waveguide is removed at the feed of horn antenna.

3.2. SIW H-Plane Sectoral Horn Lens Antenna

Figure 2(b) demonstrates the structure of the dielectric loaded SIW H-plane horn lens antenna. The rectangular waveguide, the sectoral horn antenna, the lens and the loaded dielectric are integrated in the single dielectric substrate. According to the design rule of the SIW, the spacing between two

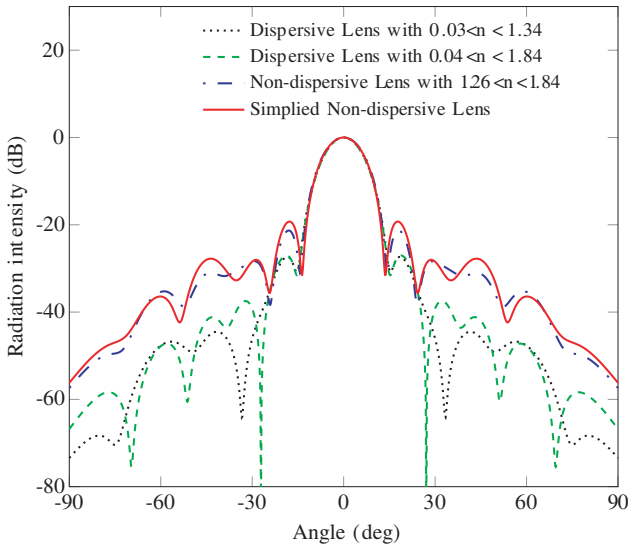

Figure 3. Far-field radiation patterns of the proposed dispersive lens antenna shown in Figure 1(c) (black dotted line), dispersive lens antenna achieved by the multiplication of the index profile Figure 1(c) with the factor 1.37 (green dashed line), non-dispersive lens antenna shown in Figure 2(a) (blue dash-dotted line), and simplified non-dispersive lens antenna achieved by replacing the index in region II of Figure 2(a) by the value of 1.84 (red solid line) at the working frequency 35 GHz.

adjacent vias (W) and the radius of the via are chosen to be 1 mm and 0.4 mm, respectively [33]. In the waveguide of the SIW horn, the dominant mode is TE_{10}. To ensure single mode excitation of the horn, the width $a^{'}$ of the SIW is determined as 4 mm using the equivalence between the SIW and conventional rectangular waveguides with solid walls [33]. The rectangular dielectric loading in front of the horn aperture can be considered as a dielectric guiding structure in the E-plane excited by the horn aperture. Through properly choosing the length of the dielectric loading, reduced beamwidth in the E-plane can be achieved.

4. SIMULATION RESULTS OF SIW H-PLANE HORN LENS ANTENNA

Using Ansoft HFSS CAD tool [34], we investigated the performance of the proposed SIW H-plane horn lens antenna. First, consider the H-plane horn lens antenna without the dielectric loading ($L_3 = 0$). In this case, the simulated radiation patterns are shown in Figure 4(a). The gain is 11.73 dB, the

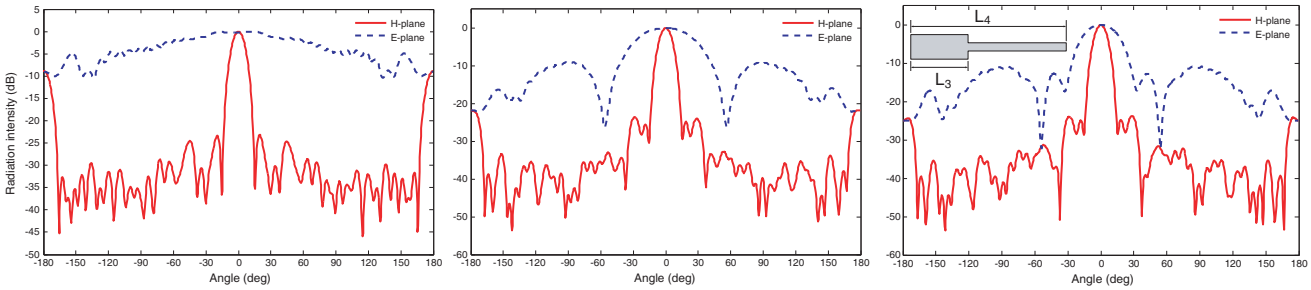

Figure 4. Radiation patterns of the SIW horn lens antenna (a) without dielectric loading. ($L_3 = 0$) (b) with rectangular dielectric loading ($L_3 = 7.1$ mm) (c) with modified dielectric loading ($L_3 = 7.1$ mm and $L_4 = 28$ mm), the inset shows the cross section of the modified dielectric loading.

half-power beamwidths of the E-plane (z-y plane) and the H-plane (z-x plane) are 139.8° and 11.7°, respectively. The peak sidelobe ratio in the front H-plane pattern ($-90° \leqslant \theta \leqslant 90°$) is -23.17 dB. The high-gain and low sidelobe level performance of the H-plane radiation verify the success of the proposed implementation approach.

A rectangular dielectric loading is now placed in front of the aperture of the horn. Simulation results indicate that by increasing the length of dielectric loading the half-power beamwidth in the H-plane is almost constant, approximately 12°. The E-plane HPBW decreases with an increase in the dielectric length; however, this leads to producing sidelobes in the E-plane, their level increasing for lengths more than 4 mm. Therefore, through properly choosing the length of the dielectric loading, more directive pattern in the E-plane can be achieved. For example, the simulated radiation patterns when the length of the dielectric loading L_3 is 7.1 mm are shown in Figure 4(b). In this case, the gain of the antenna is 15.88 dB, and the E- and H-plane HPBWs are 52.6° and 11.6°, respectively. The PSLR in the front H-plane pattern is -23.63 dB and in the E-plane is -9.2 dB.

Some improvement for the patter in the E-plane can be obtained if the cross section of the loading region varies as shown in the inset of Figure 4(c) (this geometry can also be made by constructing the substrate with three layers, where the middle dielectric slab is of greater length L_4). The radiation patterns of the antenna with modified dielectric loading with $L_3 = 7.1$ mm and $L_4 = 28$ mm are shown in Figure 4(c). In this case, the gain of the antenna is 17.79 dB. The HPBW, first sidelobe level (SLL) and PSLR in the E-plane are 33.2°, -12.65 dB and -10.72 dB, respectively. It is worthy of noting that the radiation pattern in the H-plane does not change considerably with variation of the length of the middle dielectric slab.

The SIW H-plane horn antenna loaded with rectangular dielectric but without the drilled array holes is also investigated. Its far field radiation patterns, with the dielectric length equal to 7.1 mm, is shown in Figure 5. The gain is found to be 10.2 dB. It is obvious from the simulation results that by using the proposed designed lens and the dielectric loading, the radiation patterns are improved in the H- and E-plane and consequently, higher directivity has been achieved.

As shown in Figure 2(b), a coaxial probe has been used for excitation of TE_{10} mode of the waveguide. The radii of the prob and the outer shield of the coaxial feed are $R_1 = 0.25$ mm and $R_2 = 0.5$ mm, respectively. The distance of the probe location to the shorted end of the waveguide is optimized with respect to impedance matching and the value of $L_p = 1.23$ mm has been chosen. The simulated S_{11} versus frequency for the rectangular dielectric loaded antenna with $L_3 = 7.1$ mm is given in Figure 6.

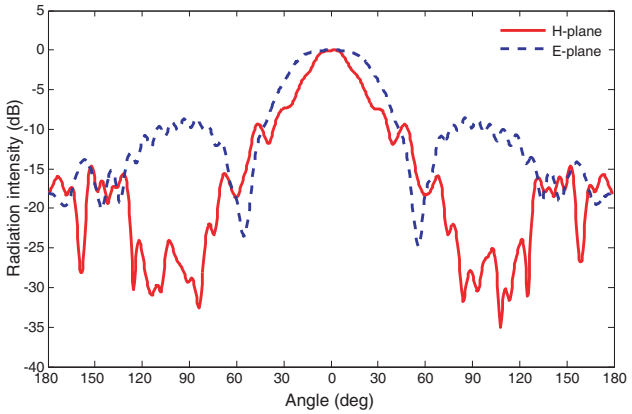

Figure 5. Radiation patterns of the rectangular dielectric loaded SIW horn antenna without drilled hole arrays ($L_3 = 7.1$ mm).

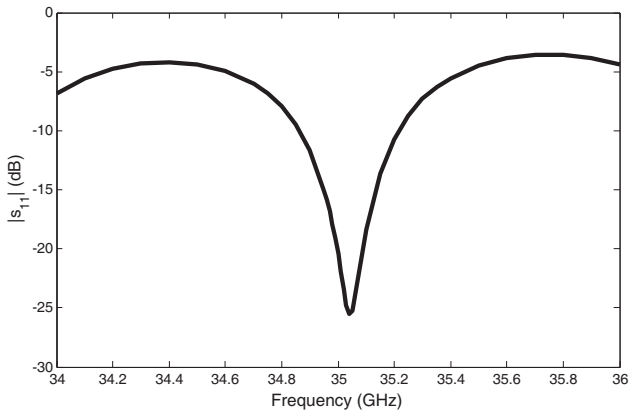

Figure 6. Simulated $|S_{11}|$ of the rectangular dielectric loaded SIW horn lens antenna ($L_3 = 7.1$ mm).

5. DESIGN OF A HIGH GAIN, LOW SIDELOBE ANTENNA BASED ON MAXWELL-FISHEYE LENS

The Maxwell-fish-eye lens is a gradient refractive index device formed from a radial distribution of index expressed as:

$$n'(\xi,\eta) = \frac{n_0}{1+(\frac{r}{R})^2} \tag{9}$$

where n_0 denotes the index of refraction at the center of the lens, and R is the radius of the lens [35]. In our design, we consider $n_0 = 1$, $R = 43$ mm and the operating frequency as 39 GHz. The essential feature of this lens is that the rays emanating from a line source on the lens surface focus to a conjugate point on the opposite side of the lens. Since the quasi-cylindrical waves produced by the line source are transformed into plane waves in the middle of the lens, it can be inferred that we can partially use this index distribution to design a high-gain lens antenna [22]. For design of the desired lens antenna, consider Figure 7(a) in which we have chosen $R = 43$ mm. The index distribution in region I is defined according to Equation (9) and in region II and III is equal to unity. This figure is mapped quasi-conformally to a physical region shown in Figure 7(b) in which the curved region is flattened. The mapping can be obtained by solving the following Laplace's equations for analytical functions $x(\xi,\eta)$ and $y(\xi,\eta)$ in the virtual space:

$$x_{\xi\xi} + x_{\eta\eta} = 0, \qquad y_{\xi\xi} + y_{\eta\eta} = 0, \tag{10}$$

subject to the following boundary conditions:

$$x|_{AB} = -86, \quad x|_{CD} = 86, \quad n.\nabla x|_{BC,AD} = 0, \tag{11}$$

$$y|_{BC} = -29.3, \quad y|_{AD} = 5.7, \quad n.\nabla y|_{AB,CD} = 0. \tag{12}$$

In this case, the anisotropic components corresponding to the quasi-conformal transformation can be neglected, and thus, the medium is approximated by an isotropic dielectric $n(x,y) = n'(\xi,\eta)/\sqrt{x_\xi^2 + x_\eta^2}$. The distribution of the refractive index for the physical domain is shown in Figure 7(b). We have chosen the refractive index distribution in the region enclosed by the black dashed line as the profile of the proposed lens. It is seen that the index varies between 0.2 and 1.14. In order to implement the designed lens using GPCs in the host medium with a dielectric constant of 3.38, all the refractive index values of the lens profile are multiplied by 1.61 (1.84/1.14), and next, all the less-than 1.26 values are replaced by 1.26. The obtained non-dispersive refractive index profile is shown in Figure 8(a).

The performance of the proposed lens antennas has been investigated. Simulation results for the far-field radiation patterns in Figure 9 show that the main lobes are slightly widened through such simplifications, however, high-gain performance of the designed lens is still preserved. The half-power beamwidth and peak sidelobe ratio of the non-dispersive lens antenna are 11.17° and −19.1 dB, respectively.

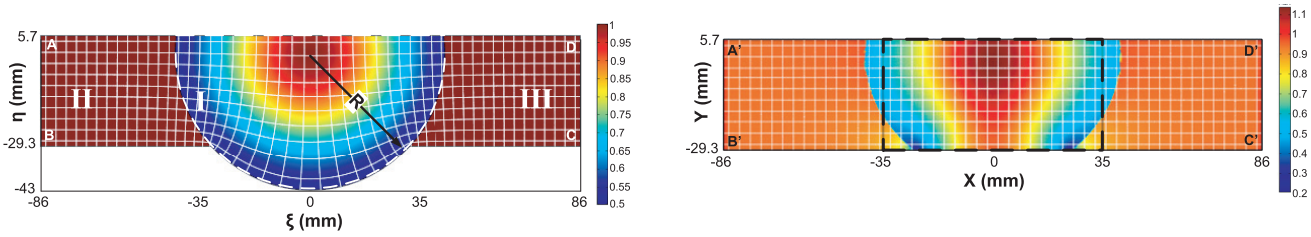

(a) (b)

Figure 7. Quasi-conformal mapping between (a) virtual, and (b) physical space indicating the refractive index resulting from the mapping. The refractive index distribution in the region enclosed by the black dashed line is chosen as the proposed lens.

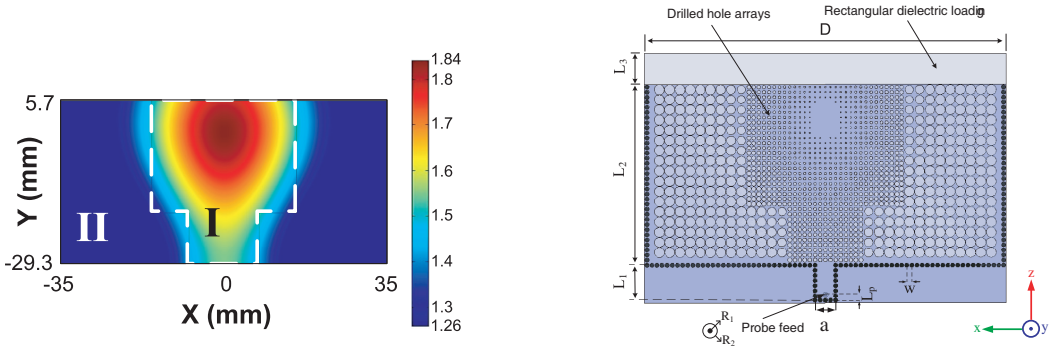

Figure 8. (a) Refractive index distribution of the simplified lens which is used in the implementation of the SIW Maxwell-fisheye-based lens antenna. (b) Structure of SIW Maxwell-fisheye-based lens antenna with a rectangular dielectric loading. $W = 1\,\text{mm}$, $a^{'} = 4\,\text{mm}$, $L_1 = 7\,\text{mm}$, $L_2 = 35\,\text{mm}$, $L_3 = 6\,\text{mm}$, $L_p = 1.1\,\text{mm}$, $D = 71\,\text{mm}$, $R_2 = 0.5\,\text{mm}$, $R_1 = 0.25\,\text{mm}$. The thickness of the dielectric substrate is 2.439 mm.

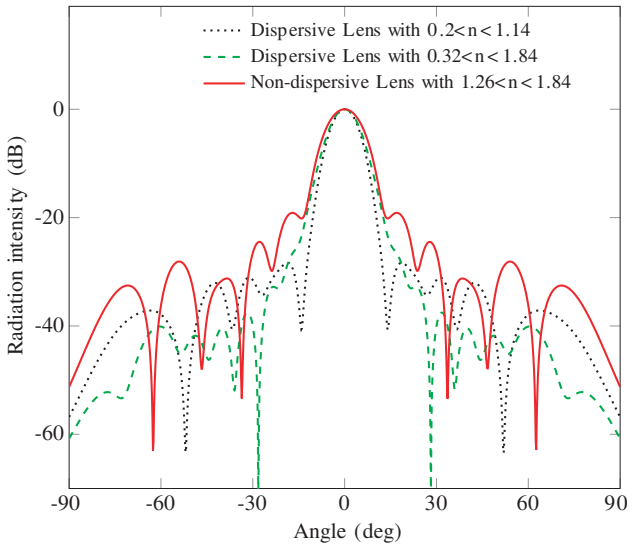

Figure 9. Far-field radiation patterns of the proposed dispersive lens antenna shown in Figure 7(b) (black dotted line), dispersive lens antenna achieved by the multiplication of the index profile Figure 7(b) with the factor 1.61 (green dashed line), and non-dispersive lens antenna shown in Figure 8(a) (red solid line) at the working frequency 39 GHz.

6. LENS ANTENNA IMPLEMENTATION

As with the horn lens antenna, this lens can also be implemented using graded photonic crystals and the SIW technology. As can be seen in Figure 8(a), the refractive index varies largely in region I as the main part of the lens and smoothly around 1.26 in most parts of region II. Therefore, for further simplification of the lens implementation, we use GPCs with the lattice constant being 1 mm in region I, and 2 mm in region II, respectively, as shown in Figure 8(b). This figure demonstrates the structure of the dielectric loaded SIW lens antenna. The rectangular waveguide, the lens and the loaded dielectric are integrated in a single dielectric substrate.

7. SIMULATION RESULTS OF SIW MAXWELL-FISHEYE-BASED LENS ANTENNA

The performance of the proposed SIW lens antenna is investigated using Ansoft HFSS. First, consider the case without the dielectric loading ($L_3 = 0$). The simulated radiation patterns are shown in Figure 10(a). In this case, the gain is 13.88 dB, the E- and H-plane HPBWs are 125.6° and 10.3°, respectively. The PSLR of the front H-plane pattern ($-90° \leqslant \theta \leqslant 90°$) is -23.24 dB.

A rectangular dielectric loading is now placed in front of the aperture of the antenna. As in the previous case, simulation results reveal that the radiation pattern in the E-plane can become more directive by properly choosing the length of the dielectric loading. For the length of the rectangular dielectric equal to 6 mm, the simulated radiation patterns are plotted in Figure 10(b). In this case, the antenna gain is 17.1 dB and the E- and H-plane HPBWs are 55.5° and 10.8°, respectively. The PSLR in the front H-plane is -17.1 dB and in the E-plane is -8.72 dB.

The effect of modifying the dielectric loading in the same way as done in horn antenna is also investigated. Figure 10(c) shows the radiation patterns of the antenna with $L_3 = 6$ mm and $L_4 = 26$ mm. In this case, the gain of the antenna is 19.53 dB. The HPBW, first sidelobe level and PSLR in the E-plane are 32.5°, -12.68 dB and -11.15 dB, respectively.

The rectangular dielectric loaded SIW antenna without the drilled array holes is also investigated, where its radiation pattern is shown in Figure 11. It is seen that the pattern is not satisfactory in the

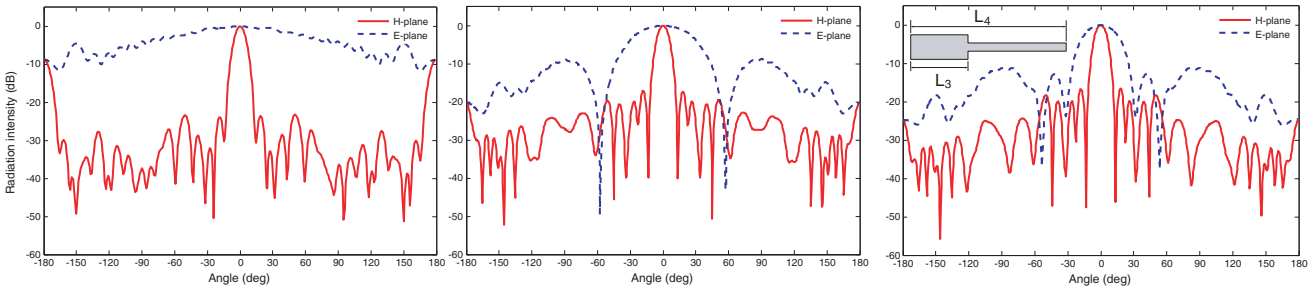

Figure 10. Radiation patterns of the SIW Maxwell-fisheye-based lens antenna. (a) Without dielectric loading. ($L_3 = 0$), (b) with rectangular dielectric loading ($L_3 = 6$ mm), (c) with a modified dielectric loading ($L_3 = 6$ mm and $L_4 = 26$ mm), the inset shows the cross section of the modified dielectric loading.

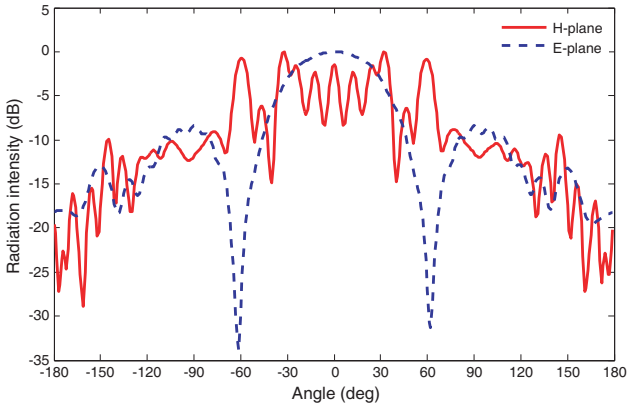

Figure 11. Radiation patterns of the rectangular dielectric loaded SIW antenna without drilled hole arrays ($L_3 = 6$ mm).

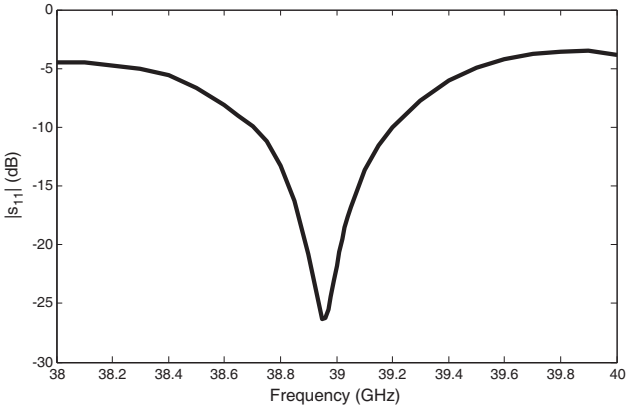

Figure 12. Simulated $|S_{11}|$ of the rectangular dielectric loaded SIW Maxwell-fisheye-based lens antenna ($L_3 = 6$ mm).

H-plane. Thus, the improvement obtained by applying the proposed design is evident. The simulated S_{11} versus frequency for the rectangular dielectric loaded antenna with $L_3 = 6\,\text{mm}$ is given in Figure 12.

8. CONCLUSION

Conformal and quasi-conformal transformations are used to design high-gain H-plane horn and Maxwell-fisheye-based lens antennas, which can be realized using gradient-index materials. By applying proper simplifying techniques, the designed lenses can be implemented by graded photonic crystals and the SIW technology on a single substrate. The simulation results demonstrate high performance of the proposed SIW lens antennas and confirm the validity of our proposal in combining the features of transformation optics and the SIW technology.

REFERENCES

1. Pendry, J. B., D. Schuring, and D. R. Smith, "Controlling electromagnetic fields," *Science*, Vol. 312, No. 5781, 1780–1782, 2006.
2. Leonhardt, U., "Optical conformal mapping," *Science*, Vol. 312, No. 5781, 1777–1780, 2006.
3. Schurig, D., J. J. Mock, B. J. Justice, S. A. Cummer, J. B. Pendry, A. F. Starr, and D. R. Smith, "Metamaterial electromagnetic cloak at microwave frequencies," *Science*, Vol. 314, No. 5801, 977–980, 2006.
4. Cai, W., U. K. Chettiar, A. V. Kildishev, and V. M. Shalaev, "Optical cloaking with metamaterials," *Nat. Phot.*, Vol. 1, 224–227, 2007.
5. Wang, W., L. Lin, X. Yang, J. Cui, C. Du, and X. Luo, "Design of oblate cylindrical perfect lens using coordinate transformation," *Opt. Express*, Vol. 16, 8094–8105, 2008.
6. Tsang, M. and D. Psaltis, "Magnifying perfect lens and superlens design by coordinate transformation," *Phys. Rev. B*, Vol. 77, 035122, 2008.
7. Rahm, M., D. Schurig, D. A. Roberts, S. A. Cummer, D. R. Smith, and J. B. Pendry, "Design of electromagnetic cloaks and concentrators using form-invariant coordinate transformations of Maxwell's equations," *Photonics Nanostruct. Fundam. Appl.*, Vol. 6, No. 1, 87–95, 2008.
8. Kong, F., B.-I. Wu, J. A. Kong, J. Huangfu, S. Xi, and H. Chen, "Planar focusing antenna design by using coordinate transformation technology," *Appl. Phys. Lett.*, Vol. 91, 253509, 2007.
9. Jiang, W. X., T. J. Cui, H. F. Ma, X. M. Yang, and Q. Cheng, "Layered high-gain lens antennas via discrete optical transformation," *Appl. Phys. Lett.*, Vol. 83, 221906, 2008.
10. Luo, Y., J. Zhang, H. Chen, J. Huangfu, and L. Ran, "High-directivity antenna with small antenna aperture," *Appl. Phys. Lett.*, Vol. 95, 193506, 2009.
11. Tichit, P.-H., S. N. Burokur, and A. de Lustrac, "Design and experimental demonstration of a high-directive emission with transformation optics," *Phys. Rev. B*, Vol. 83, No. 15, 155108, 2011.
12. Tichit, P. -H., S. N. Burokur, and A. de Lustrac, "Transformation media producing quasi-perfect isotropic emission," *Optics Express*, Vol. 19, No. 21, 20551–20556, 2011.
13. Leonhardt, U. and T. G. Philbin, "Transformation optics and the geometry of light," *Prog. Opt.*, Vol. 53, 69–152, 2009.
14. Li, J. and J. B. Pendry, "Hiding under the carpet: A new strategy for cloaking," *Phys. Rev. Lett.*, Vol. 101, No. 20, 203901, 2008.
15. Ma, Y. G., N. Wang, and C. K. Ong, "Application of inverse, strict conformal transformation to design waveguide devices," *J. Opt. Soc. Amer. A*, Vol. 27, No. 5, 968–972, 2010.
16. Liu, R., C. Ji, J. J. Mock, J. Y. Chin, T. J. Cui, and D. R. Smith, "Broadband ground-plane cloak," *Science*, Vol. 323, No. 5912, 366–369, 2009.
17. Smith, D. R., Y. Urzhumov, N. B. Kundtz, and N. I. Landy, "Enhancing imaging systems using transformation optics," *Optics Express*, Vol. 18, No. 20, 21238–21251, 2010.
18. Kundtz, N. and D. R. Smith, "Extreme-angle broadband metamaterial lens," *Nat. Mater.*, Vol. 9, No. 12, 129–132, 2010.

19. Mei, Z. L., J. Bai, and T. J. Cui, "Experimental verification of a broadband planar focusing antenna based on transformation optics," *New J. Phys.*, Vol. 13, No. 6, 063028, 2011.
20. Garcia-Meca, C., A. Martnez, and U. Leonhardt, "Engineering antenna radiation patterns via quasi-conformal mappings," *Optics Express*, Vol. 19, No. 24, 23743–23750, 2011.
21. Aghanejad, I., H. Abiri, and A. Yahaghi, "Design of high-gain lens antenna by gradient-index metamaterials using transformation optics," *IEEE Trans. Antennas propag.*, Vol. 60, No. 9, 4074–4081, 2012.
22. Aghanejad, I., H. Abiri, A. Yahaghi, and R. Ramezani, "A high-gain lens antenna based on transformation optics," *Loughborough Antennas and Propag. Conf.*, 1–4, Loughborough, UK, Nov. 2012.
23. Bozzi, M., A. Georgiadis, and K. E. Wu, "Review of substrate-integrated waveguide circuits and antennas," *IET Microw. Antennas propag.*, Vol. 5, No. 8, 909–920, 2011.
24. Yan, L., W. Hong, G. Hua, J. Chen, K. Wu, and T. J. Cui, "Simulation and experiment on SIW slot array antennas," *IEEE Microw. Wirel. Compon. Lett.*, Vol. 14, No. 9, 446–448, 2004.
25. Xu, F., K. Wu, and X. Zhang, "Periodic leaky-wave antenna for millimeter wave applications based on substrate integrated waveguide," *IEEE Trans. Antennas Propag.*, Vol. 58, No. 2, 340–347, 2010.
26. Cheng, Y. J., W. Hong, and K. Wu, "Design of a monopulse antenna using a dual V-type linearly tapered slot antenna (DVLTSA)," *IEEE Trans. Antennas Propag.*, Vol. 56, No. 9, 903–2909, 2008.
27. Awida, M. H. and A. E. Fathy, "Substrate-integrated waveguide Ku-band cavity-backed 2×2 microstrip patch array antenna," *IEEE Antennas Wirel. Propag. Lett.*, Vol. 8, 1054–1056, 2009.
28. Wang, H., D.-G. Fang, B. Zhang, and W.-Q. Che, "Dielectric loaded substrate integrated waveguide (SIW) H-plane horn antennas," *IEEE Trans. Antennas Propag.*, Vol. 58, No. 3, 640–647, 2010.
29. Henrici, P., *Applied and Computational Complex Analysis*, Vol. 3, Wiley, 1986.
30. [Online], Available: http://www.comsol.com.
31. Vasic, B., G. Isic, R. Gajic, and K. Hingerl, "Controlling electromagnetic fields with graded photonic crystals in metamaterial regime," *Optics Express*, Vol. 18, No. 19, 20321–20333, 2010.
32. Halevi, P., A. A. Krokhin, and J. Arriaga, "Photonic crystal optics and homogenization of 2D periodic composites," *Phys. Rev. Lett.*, Vol. 82, No. 4, 719–722, 1999.
33. Che, W., K. Deng, D. Wang, and Y. L. Chow, "Analytical equivalence between substrate-integrated waveguide and rectangular waveguide," *IET Microw. Antennas Propag.*, Vol. 2, No. 1, 35–41, 2008.
34. [Online], Available: http://www.ansys.com/.
35. Marchand, E. W., *Gradient Index Optics*, Academic Press, New York, 1978.